

Supporting Information

Ultralow lattice thermal conductivity and improved thermoelectric performance in a Hf-free half-Heusler compound modulated by entropy engineering

Xiaoling Zhang^a, Ming Huang^a, Hongjun Li^a, Jiaxin Chen^b, Pengfei Xu^c, Biao Xu^c,
Yifeng Wang^b, Guodong Tang^{a,*}, Sen Yang^{a,*}

^a School of Materials Science and Engineering, Nanjing University of Science and
Technology, Nanjing 210094, P. R. China

^b College of Materials Science and Engineering, Nanjing Tech University, Nanjing
210009, P. R. China

^c School of Chemistry and Chemical Engineering, Nanjing University of Science and
Technology, Nanjing 210094, P. R. China

*Corresponding Authors: yangsen@njust.edu.cn (Prof. S. Yang)

tangguodong@njust.edu.cn (Prof. G. D. Tang)

1. Single parabolic band (SPB) modeling

The density-of-states effective mass m_d^* is determined by eqs. (S1-S3):¹

$$S = \frac{k_B}{e} \left(\frac{(2+\lambda)F_{\lambda+1}(\eta)}{(1+\lambda)F_\lambda(\eta)} - \eta \right) \quad (\text{S1})$$

$$n_H = \frac{(2m_d^*k_B T)^{3/2}}{3\pi^2\hbar^3} \frac{(\lambda+1)^2 F_\lambda^2(\eta)}{(2\lambda+1/2)F_{(2\lambda-1/2)}(\eta)} \quad (\text{S2})$$

$$F_j(\eta) = \int_0^\infty \frac{\epsilon^j d\epsilon}{1 + \exp(\epsilon - \eta)} \quad (\text{S3})$$

$$L = \frac{k_B^2}{e^2} \frac{(1+\lambda)(3+\lambda)F_\lambda(\eta)F_{\lambda+2}(\eta) - (2+\lambda)^2 F_{\lambda+1}^2(\eta)}{(1+\lambda)^2 F_\lambda^2(\eta)} \quad (\text{S4})$$

Where S is the Seebeck coefficient, k_B is the Boltzmann constant (about 1.38×10^{-23} J K⁻¹), e is the elementary charge (about 1.6×10^{-19} C), λ is the scattering factor ($\lambda = 0$ for acoustic phonon scattering or alloy scattering), ϵ is the reduced carrier energy, η is the reduced Fermi energy ($E_F/k_B T$), $F_j(\eta)$ is the Fermi-Dirac integrals of order j , n_H is the Hall carrier concentration, T is the Kelvin temperature, \hbar is the reduced Planck constant (about 1.05×10^{-34} J s) and L is the Lorenz number. The reduced Fermi energy η can be estimated from the measured Seebeck coefficient S . Thus, the determination of the reduced Fermi energy η and the measured Hall carrier concentration n_H allows the calculation of the density-of-states effective mass m_d^* .

2. Calculations of the E_{def} and E_{al} based on the SPB model

The Hall factor r_H is given as:¹

$$r_H = \frac{3}{2} F_{1/2}(\eta) \frac{\left(\frac{1}{2}+2\lambda\right)F_{2\lambda-1/2}(\eta)}{(1+\lambda)^2 F_\lambda^2(\eta)} \quad (\text{S5})$$

and¹

$$\mu_H = \mu r_H \quad (\text{S6})$$

Where μ_H is the Hall carrier mobility, μ is the drift mobility. While half-Heusler compound TiNiSn is considered as one type of polar semiconductors,² only the non-

polar scattering process is taken into account because of the high carrier concentration range for samples with increased ΔS_{conf} .^{3,4} The scattering by acoustic vibrations is:^{4,5}

$$\mu^{ph} = \frac{2^{1/2}\pi e \hbar^4}{3(k_B T)^{3/2}} \frac{v_l^2 \rho}{E_{\text{def}}^2 (m_b^*)^{3/2} m_I^*} \frac{F_0(\eta)}{F_{1/2}(\eta)} \quad (\text{S7})$$

Where v_l is the longitudinal phonon velocity, ρ is the mass density, E_{def} is the deformation potential coefficient, m_b^* is the band effective mass, it can be calculated from $m_d^* = N_v^{2/3} m_b^*$, m_I^* is the inertial effective mass (for isotropic band, $m_I^* = m_b^*$).⁶⁻⁸ The scattering by alloying atoms is:^{4,9}

$$\mu^{al} = \frac{16e \hbar^4}{9\sqrt{2}\pi x(1-x)(k_B T)^{1/2}} \frac{N_0}{E_{\text{al}}^2 (m_b^*)^{3/2} m_I^*} \frac{F_0(\eta)}{F_{1/2}(\eta)} \quad (\text{S8})$$

Where N_0 is the number of atoms per unit volume, x is the fractional concentration, E_{al} is the alloy scattering potential. By using the Matthiessen's rule, the drift mobility μ can be written as:^{4,10}

$$\frac{1}{\mu} = \frac{1}{\mu^{ph}} + \frac{1}{\mu^{al}} \quad (\text{S9})$$

3. Calculation of the weighted mobility μ_W

The weighted mobility μ_W at a certain temperature is calculated from:¹¹

$$\mu_W = \frac{3h^3\sigma}{8\pi e(2m_e k_B T)^{3/2}} \left[\frac{\exp\left[\frac{|S|}{k_B/e} - 2\right]}{1 + \exp\left[-5\left(\frac{|S|}{k_B/e} - 1\right)\right]} + \frac{\frac{3}{\pi^2} \frac{|S|}{k_B/e}}{1 + \exp\left[5\left(\frac{|S|}{k_B/e} - 1\right)\right]} \right] \quad (\text{S10})$$

Where h is the Planck constant (about 6.626×10^{-34} J s), σ is the electrical conductivity, m_e is the rest mass of an electron (about 9.109×10^{-31} kg).

4. Callaway–Klemens modeling

This model is based on the assumption that only the Umklapp and point defect scattering are taken into account at high temperatures ($T > \theta_D$).¹² The formula of the lattice thermal conductivity of material with point imperfections (κ_L^P) divided by the

lattice thermal conductivity of pure material (κ_L^0) is given as:¹²

$$\frac{\kappa_L^P}{\kappa_L^0} = \frac{\tan^{-1}(u)}{u} \quad (\text{S11})$$

Where u can be calculated from:¹²

$$u^2 = \frac{\pi^2 \theta_D \Omega_0}{h v_s^2} \kappa_L^0 \Gamma \quad (\text{S12})$$

Where θ_D is the Debye temperature, Ω_0 is the atomic volume, v_s is the average phonon velocity. According to the theory developed by Slack¹³ and Abeles,¹⁴ the disorder scattering parameter Γ in eq. (S12) contains two parts, i.e., $\Gamma = \Gamma_M + \Gamma_S$, for which Γ_M represents the disorder scattering due to mass fluctuations and Γ_S represents the disorder scattering due to strain field fluctuations. More specifically, the Γ_M is given as:¹⁵

$$\Gamma_M = \frac{\sum_{i=1}^n c_i \left(\frac{\bar{M}_i}{\bar{M}} \right)^2 \Gamma_M^i}{(\sum_{i=1}^n c_i)} \quad (\text{S13})$$

the computation formulae of several parameters in eq. (S13) are as follows:¹⁵

$$\bar{M}_i = \sum_k f_j^k M_j^k \quad (\text{S14})$$

$$\bar{M} = \frac{\sum_{i=1}^n c_i \bar{M}_i}{(\sum_{i=1}^n c_i)} \quad (\text{S15})$$

$$\Gamma_M^i = \sum_k f_j^k \left(1 - \frac{M_j^k}{\bar{M}_i} \right)^2 \quad (\text{S16})$$

Take ‘Ti_{0.6}Zr_{0.4}NiSn_{0.98}Sb_{0.02}’ for example, $c_1 + c_2 + c_3 = 3$, $\bar{M}_1 = 0.6 \times 47.88 + 0.4 \times 91.22 = 65.216$, $\bar{M}_3 = 0.98 \times 118.69 + 0.02 \times 121.75 = 118.7512$, $\bar{M} = \frac{1}{3}(\bar{M}_1 + M_{Ni} + \bar{M}_3) \approx 80.8857$, $\Gamma_M = \frac{1}{3}\{(65.216/80.8857)^2 \times [0.6 \times (1 - 47.88/65.216)^2 + 0.4 \times (1 - 91.22/65.216)^2] + (118.7512/80.8857)^2 \times [0.98 \times (1 - 118.69/118.7512)^2 + 0.02 \times (1 - 121.75/118.7512)^2]\} \approx 0.02298$ (the atomic weights are listed in Table S3).

The Γ_S is given as:^{14,15}

$$\Gamma_S = \frac{\sum_{i=1}^n c_i \left(\frac{M_i}{M}\right)^2 \Gamma_S^i}{\left(\sum_{i=1}^n c_i\right)} \quad (\text{S17})$$

$$\Gamma_S^i = \varepsilon_i \sum_k f_j^k \left(1 - \frac{r_j^k}{\bar{r}_i}\right)^2 \quad (\text{S18})$$

$$\bar{r}_i = \sum_k f_j^k r_j^k \quad (\text{S19})$$

Take ‘Ti_{0.6}Zr_{0.4}NiSn_{0.98}Sb_{0.02}’ for example, $\bar{r}_1 = 0.6 \times 1.46 + 0.4 \times 1.57 = 1.504$, $\bar{r}_3 = 0.98 \times 1.40 + 0.02 \times 1.41 = 1.4002$ (this term can be ignored), $\Gamma_S = \frac{1}{3} \left\{ (65.216/80.8857)^2 \times \varepsilon_1 \times \left[0.6 \times (1 - 1.46/1.504)^2 + 0.4 \times \left(1 - \frac{1.57}{1.504}\right)^2 \right] \right\}$ (the atomic radii are listed in Table S3). The ε_i in eq. (S18) is termed as strain field factor, linked with the Grüneisen parameter γ . It is a factor that can be served as an adjustable parameter to make the theoretical prediction fit in well with the experimental data.¹⁵ In this work, first of all, we set the κ_L of TiNiSn_{0.98}Sb_{0.02} as κ_L^0 . Secondly, combined with the κ_L of Ti_{0.6}Zr_{0.4}NiSn_{0.98}Sb_{0.02} (κ_L^P), the value of u can be derived. Thirdly, the theoretical Γ_S can be obtained from $\Gamma - \Gamma_M$, as well as the ε (in particular, only the fluctuations caused by the alloying atoms at the Ti site, i.e., ε_1 , are taken into consideration). Finally, we can use the same ε in the calculations of Γ_S for Ti_{0.58}Zr_{0.4}Al_{0.02}NiSn_{0.98}Sb_{0.02} and Ti_{0.57}Zr_{0.4}Al_{0.02}Ta_{0.01}NiSn_{0.98}Sb_{0.02} on the assumption that this value is independent of small changes in compositions, together with the corresponding Γ_M , the theoretical κ_L^P of abovementioned samples can be obtained respectively.

5. Debye–Cahill modeling

The minimum thermal conductivity of an amorphous solid can be written as:¹⁶

$$\kappa_{min} = \left(\frac{\pi}{6}\right)^{1/3} k_B n^{2/3} \sum_i v_i \left(\frac{T}{\theta_i}\right)^2 \int_0^{\theta_i/T} \frac{x^3 e^x}{(e^x - 1)^2} dx \quad (S20)$$

Where n is the number density of atoms, v_i represents three sound modes (one longitudinal v_l and two transverse v_t), and θ_i is given by $\theta_i = v_i(\hbar/k_B)(6\pi^2 n)^{1/3}$.

6. Diffuson-mediated thermal transport modeling

The estimated lower limit to the thermal conductivity which is based on the diffuson model is given by:¹⁷

$$\kappa_{diff} \approx 0.76 n^{\frac{2}{3}} k_B \frac{1}{3} (2v_t + v_l) \quad (S21)$$

7. Minimal thermal conductivity supported by the periodic boundary conditions

The collective equations (including acoustic and optical components) which are essential for this kind of calculation can be found in the important research work of Chen *et al.*¹⁸

Table S1. The configurational entropy of the TiNiSn-based compounds.

Composition	$\Delta S_{\text{conf}}(R)$	$\Delta S_{\text{conf}}(\text{J mol}^{-1} \text{ K}^{-1})$
TiNiSn	0	0
TiNiSn _{0.98} Sb _{0.02}	0.098	0.815
Ti _{0.6} Zr _{0.4} NiSn _{0.98} Sb _{0.02}	0.771	6.411
Ti _{0.58} Zr _{0.4} Al _{0.02} NiSn _{0.98} Sb _{0.02}	0.859	7.140
Ti _{0.57} Zr _{0.4} Al _{0.02} Ta _{0.01} NiSn _{0.98} Sb _{0.02}	0.909	7.560

Table S2. Parameters used for the electronic and thermal transport calculations.

Description and parameters	Values
Conduction band degeneracy (N_v)	3 ⁶
Bulk modulus (B)	130.67 Gpa ¹⁹
Shear modulus (G)	44.92 Gpa ¹⁹
Elastic modulus (E)	120.91 Gpa ¹⁹
Debye temperature (θ_D)	348.566 K ¹⁹
Grüneisen parameter (γ)	2.097 ¹⁹
Poisson's ratio (r)	0.346 ¹⁹
Longitudinal phonon velocity (v_l)	5098.88 m s ⁻¹ ¹⁹
Transverse phonon velocity (v_t)	2475.62 m s ⁻¹ ¹⁹
Average phonon velocity (v_s)	2781.79 m s ⁻¹ ¹⁹
Atomic volume ($\Omega_{0,1}$, Ti _{0.6} Zr _{0.4} NiSn _{0.98} Sb _{0.02})	18.245×10 ⁻³⁰ m ³
Atomic volume ($\Omega_{0,2}$, Ti _{0.58} Zr _{0.4} Al _{0.02} NiSn _{0.98} Sb _{0.02})	18.306×10 ⁻³⁰ m ³
Atomic volume ($\Omega_{0,3}$, Ti _{0.57} Zr _{0.4} Al _{0.02} Ta _{0.01} NiSn _{0.98} Sb _{0.02})	18.41×10 ⁻³⁰ m ³
Strain field factor (ϵ)	772.776
Molecular molar mass (M)	243.573 g mol ⁻¹
Number density of atoms (n , Ti _{0.57} Zr _{0.4} Al _{0.02} Ta _{0.01} NiSn _{0.98} Sb _{0.02})	5.432×10 ²⁸ m ⁻³
Number of molecular in a crystal cell (N _{cell})	4
Number of atoms in a molecular (N _{atom})	3
Number of atoms in a primitive cell (N _{unit})	3

Table S3. The ionic radii,²⁰ atomic radii,²¹ covalent radii²² and atomic weights²⁰ (scaled to the relative atomic mass, ¹²C) of alloying elements which are involved in this work.

Elements	Ionic radii (Å)	Atomic radii (Å)	Covalent radii (Å)	Atomic weights
Ti	0.68 (Ti ⁴⁺)	1.46	1.6	47.88
Zr	0.79 (Zr ⁴⁺)	1.57	1.75	91.22
Al	0.51 (Al ³⁺)	1.43	1.21	26.98
Ta	0.68 (Ta ⁵⁺)	1.43	1.70	180.95
Ni	— ²	1.24	1.24	58.69
Sn	2.94 (Sn ⁴⁻)	1.40	1.39	118.69
Sb	2.45 (Sb ³⁻)	1.41	1.39	121.75

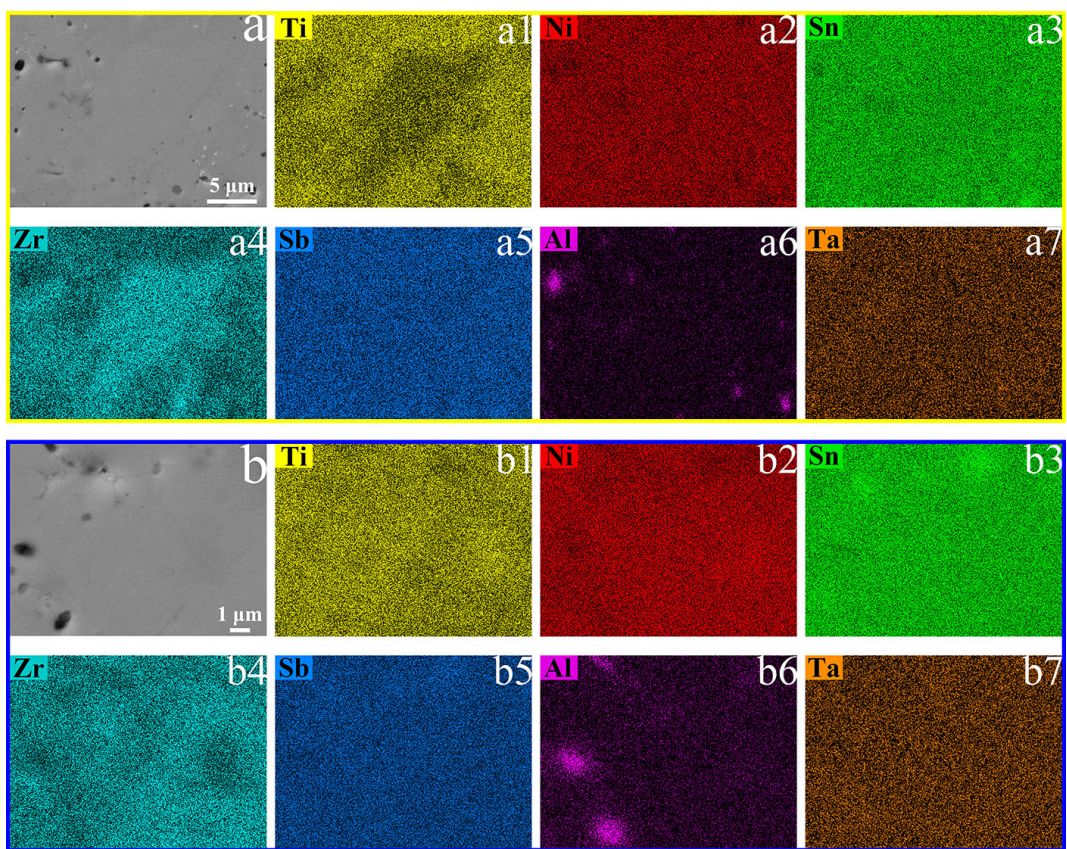


Figure S1. SEM images of polished surface for $Ti_{0.57}Zr_{0.4}Al_{0.02}Ta_{0.01}NiSn_{0.98}Sb_{0.02}$ and corresponding EDS elemental mappings, (a) low magnification, (b) high magnification.

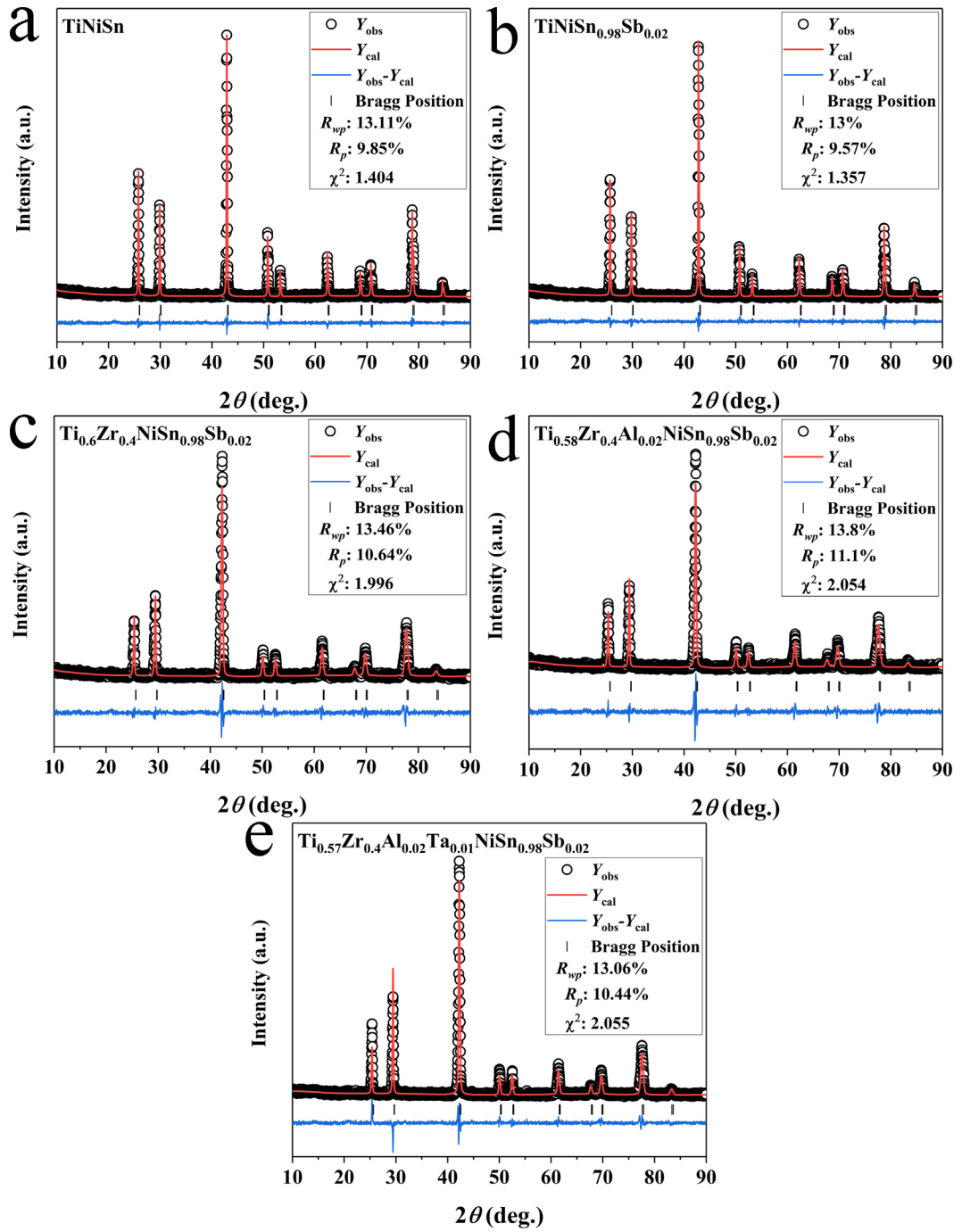


Figure S2. Rietveld refinement²³ results of (a) TiNiSn, (b) TiNiSn_{0.98}Sb_{0.02}, (c) Ti_{0.6}Zr_{0.4}NiSn_{0.98}Sb_{0.02}, (d) Ti_{0.58}Zr_{0.4}Al_{0.02}NiSn_{0.98}Sb_{0.02} and (e) Ti_{0.57}Zr_{0.4}Al_{0.02}Ta_{0.01}NiSn_{0.98}Sb_{0.02}.

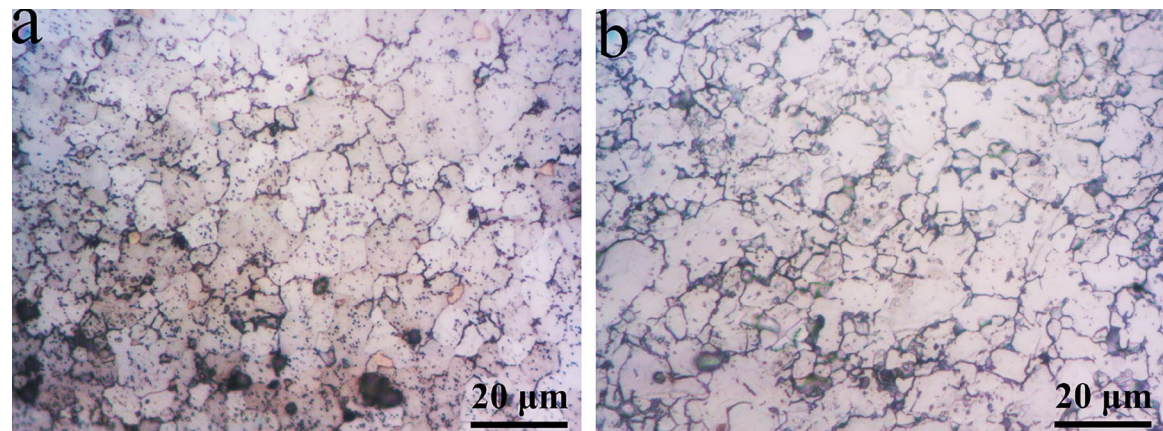


Figure S3. Comparison of the grain structure obtained from an optical microscope. (a) TiNiSn, (b) Ti_{0.57}Zr_{0.4}Al_{0.02}Ta_{0.01}NiSn_{0.98}Sb_{0.02}. The average grain size²⁴ was estimated to be about 8 μm for TiNiSn and 7.7 μm for Ti_{0.57}Zr_{0.4}Al_{0.02}Ta_{0.01}NiSn_{0.98}Sb_{0.02}.

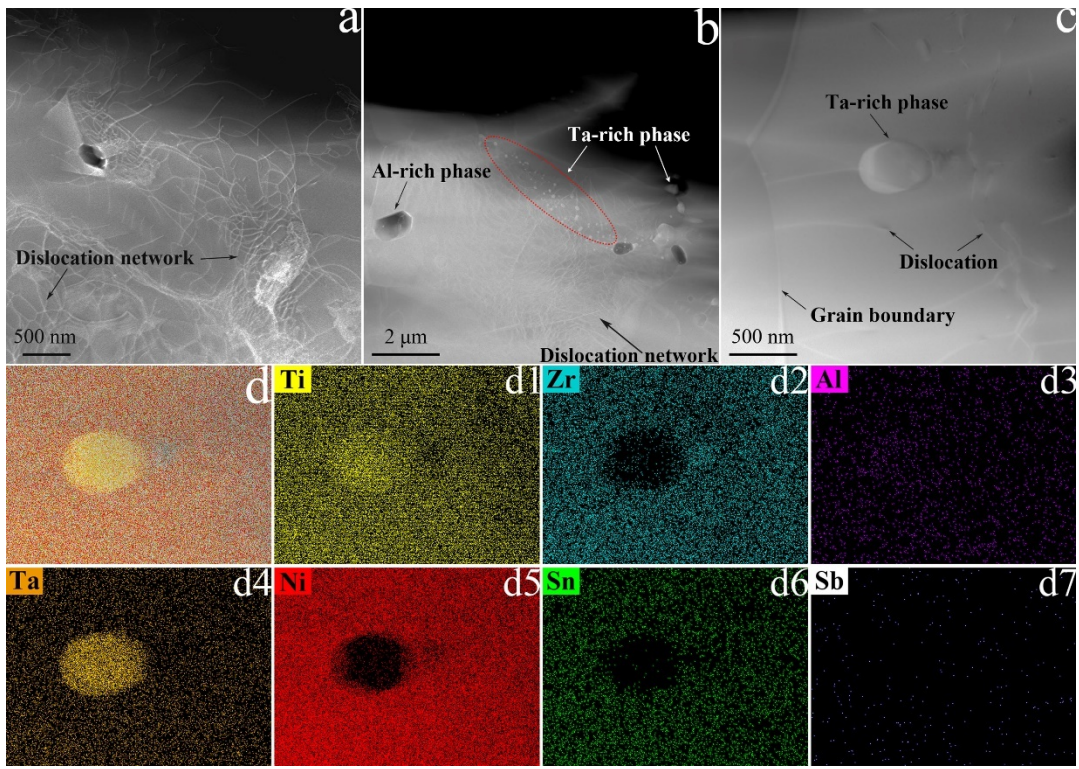


Figure S4. TEM images of $\text{Ti}_{0.57}\text{Zr}_{0.4}\text{Al}_{0.02}\text{Ta}_{0.01}\text{NiSn}_{0.98}\text{Sb}_{0.02}$. (a) Low magnification bright-field image shows dense dislocation networks exist in the matrix. (b, c) STEM-HAADF images demonstrate the existence of nanoprecipitates. (d) EDS mapping results of a selected area in (c).

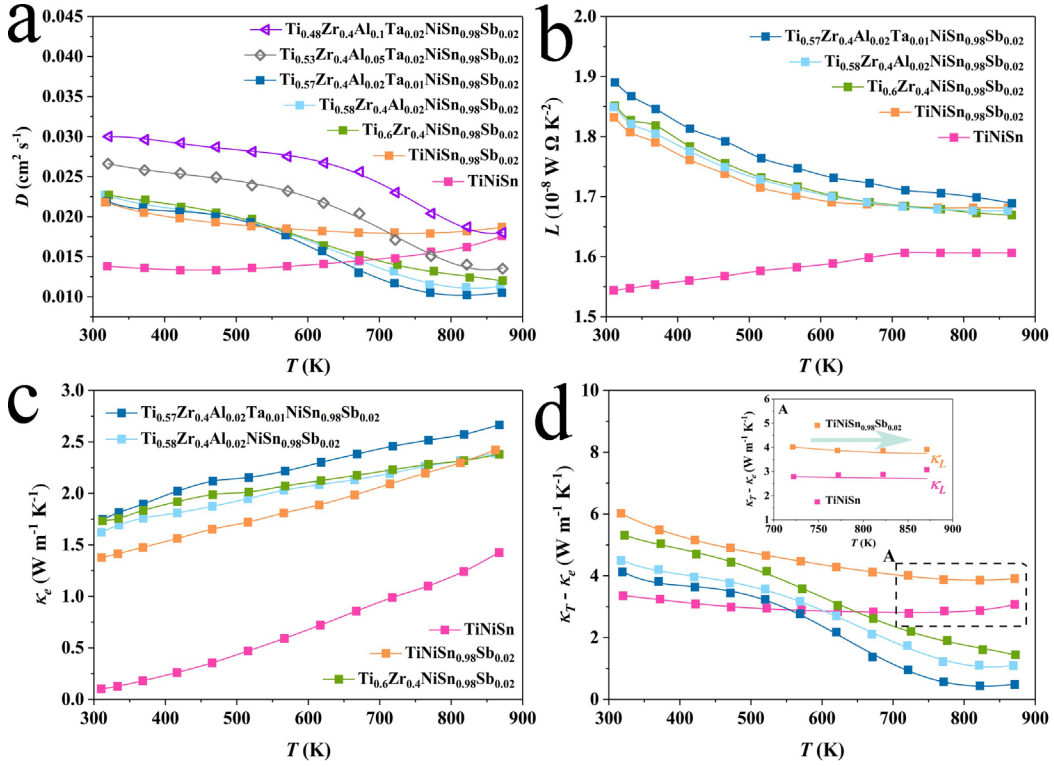


Figure S5. Temperature dependence of (a) thermal diffusivity coefficient D , (b) Lorenz number L (it was approximatively determined by the SPB model with $\lambda = 0$), (c) electronic thermal conductivity κ_e . (d) $\kappa_T - \kappa_e$.

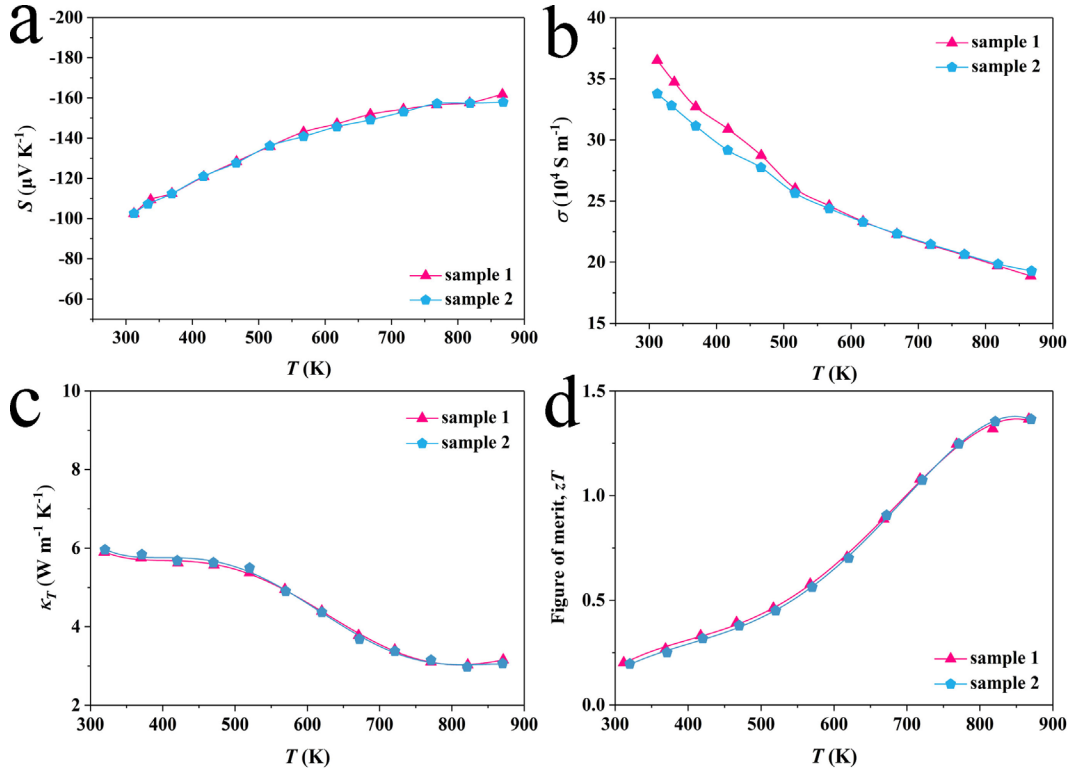


Figure S6. The repeatability test of thermoelectric performance for $\text{Ti}_{0.57}\text{Zr}_{0.4}\text{Al}_{0.02}\text{Ta}_{0.01}\text{NiSn}_{0.98}\text{Sb}_{0.02}$. Temperature-dependent (a) Seebeck coefficient, (b) electrical conductivity, (c) total thermal conductivity, (d) figure of merit, zT .

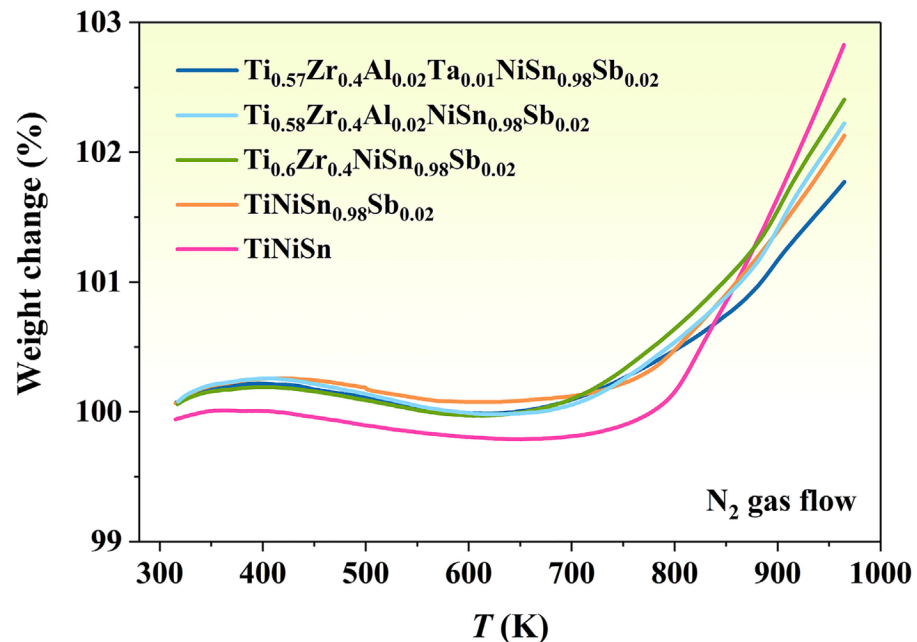


Figure S7. The thermogravimetric curves for the TiNiSn-based samples in a N₂ atmosphere up to 965 K.

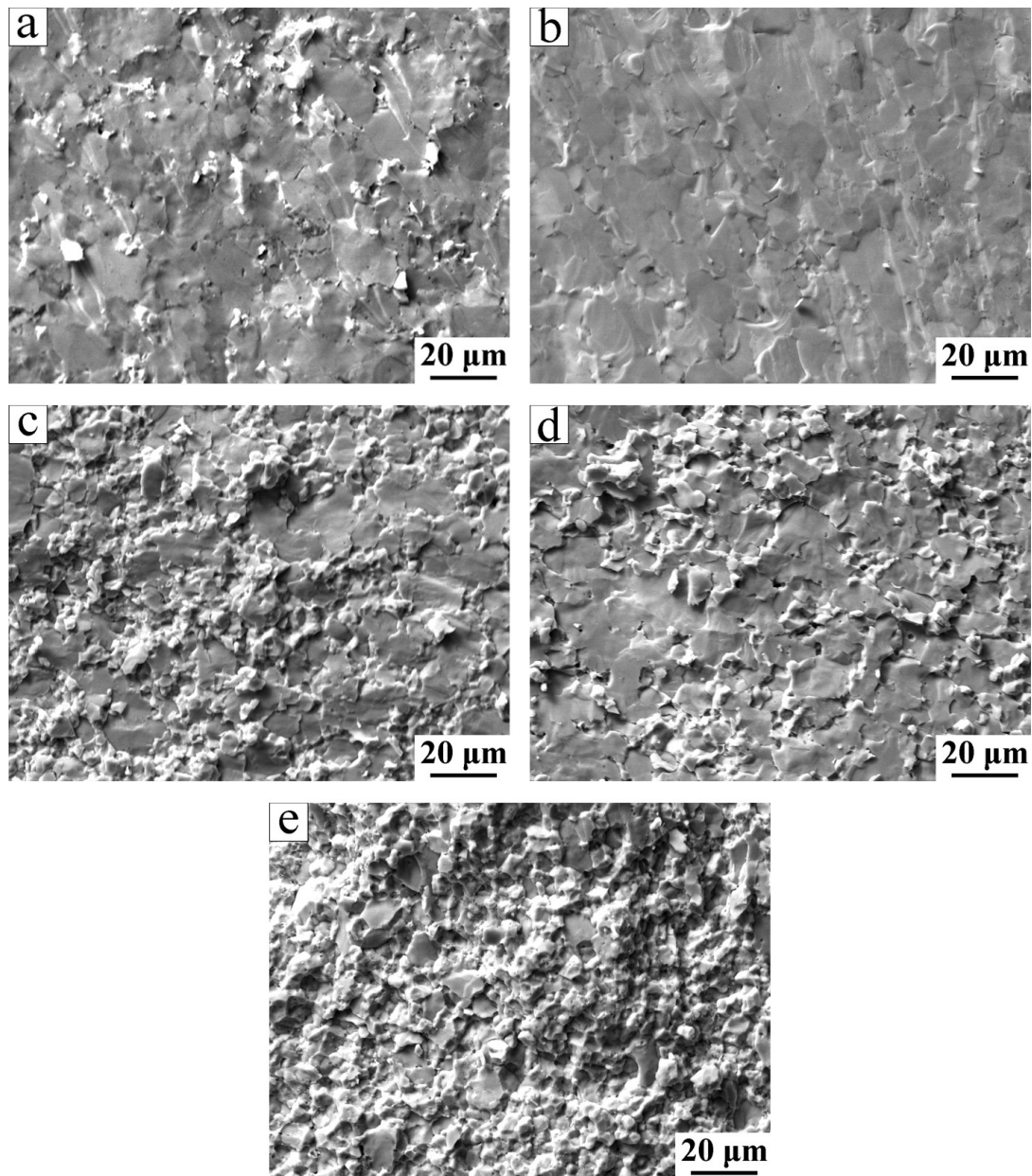


Figure S8. SEM micrographs of compression fractures for (a) TiNiSn, (b) TiNiSn_{0.98}Sb_{0.02}, (c) Ti_{0.6}Zr_{0.4}NiSn_{0.98}Sb_{0.02}, (d) Ti_{0.58}Zr_{0.4}Al_{0.02}NiSn_{0.98}Sb_{0.02}, (e) Ti_{0.57}Zr_{0.4}Al_{0.02}Ta_{0.01}NiSn_{0.98}Sb_{0.02}.

References

1. A. F. May and G. J. Snyder, in *Materials, Preparation, and Characterization in Thermoelectrics*, ed. D. M. Rowe, CRC Press, Boca Raton, Florida, 2012, ch. 11.
2. T. Graf, C. Feler and S. S. P. Parkin, *Prog. Solid State Chem.*, 2011, **39**, 1-50.
3. H. H. Xie, H. Wang, C. G. Fu, Y. T. Liu, G. J. Snyder, X. B. Zhao and T. J. Zhu, *Sci. Rep.*, 2014, **4**, 6888.
4. H. H. Xie, H. Wang, Y. Z. Pei, C. G. Fu, X. H. Liu, G. J. Snyder, X. B. Zhao and T. J. Zhu, *Adv. Funct. Mater.*, 2013, **23**, 5123-5130.
5. J. Bardeen and W. Shockley, *Phys. Rev.*, 1950, **80**, 72-80.
6. S. A. Barczak, R. J. Quinn, J. E. Halpin, K. Domosud, R. I. Smith, A. R. Baker, E. Don, I. Forbes, K. Refson, D. A. MacLaren and J.-W. G. Bos, *J. Mater. Chem. A*, 2019, **7**, 27124-27134.
7. A. Suwardi, D. Bash, H. K. Ng, J. R. Gomez, D. V. M. Repaka, P. Kumar and K. Hippalgaonkar, *J. Mater. Chem. A*, 2019, **7**, 23762-23769.
8. T. J. Zhu, Y. T. Liu, C. G. Fu, J. P. Heremans, G. J. Snyder and X. B. Zhao, *Adv. Mater.*, 2017, **29**, 1-26.
9. J. W. Harrison and J. R. Hauser, *Phys. Rev. B*, 1976, **13**, 5347-5350.
10. N. W. Ashcroft and N. D. Mermin, *Solid State Physics*, Harcourt College Publishers, Philadelphia, 1976.
11. G. J. Snyder, A. H. Snyder and M. Wood, *Adv. Mater.*, 2020, **32**.
12. J. Callaway and H. C. v. Baeyer, *Phys. Rev.*, 1960, **120**, 1149-1154.
13. G. A. Slack, *Phys. Rev.*, 1957, **105**, 829-831.
14. B. Abeles, *Phys. Rev.*, 1963, **131**, 1906-1911.
15. J. Yang, G. P. Meisner and L. D. Chen, *Appl. Phys. Lett.*, 2004, **85**, 1140-1142.
16. D. G. Cahill, S. K. Watson and R. O. Pohl, *Phys. Rev. B*, 1992, **46**, 6131-6140.
17. M. T. Agne, R. Hanus and G. J. Snyder, *Energy Environ. Sci.*, 2018, **11**, 609-616.
18. Z. W. Chen, X. Y. Zhang, S. Q. Lin, L. D. Chen and Y. Z. Pei, *Natl. Sci. Rev.*, 2018, **5**, 888-894.
19. M. Rittirum, A. Yangthaisong and T. Seetawan, *Chin. J. Phys.*, 2019, **57**, 393-402.
20. R. C. Weast, *CRC Handbook of Chemistry and Physics*, CRC Press, Boca Raton, Florida, 66th edn., 1985-1986.
21. S. L. Hoenig, *Basic Training in Chemistry*, Kluwer Academic Publishers, New York, 2002.
22. B. Cordero, V. Gómez, A. E. P.-Prats, M. Revés, J. Echeverría, E. Cremades, F. Barragán and S. Alvarez, *Dalton Trans.*, 2008, 2832-2838.
23. B. H. Toby, *J. Appl. Cryst.*, 2001, **34**, 210-213.
24. K. Shrestha, T. Yao, J. Lian, D. Antonio, M. Sessim, M. R. Tonks and K. Gofryk, *J. Appl. Phys.*, 2019, **126**, 125116.